*Sensors & Transducers Journal, Vol. 7, Special Issue, October 2009, pp. 63-77*

www.sensorsportal.com

**Sensors & Transducers**

**ISSN 1726-5479**

*http://www.sensorsportal.com*

# A Robust Miniature Silicon Microphone Diaphragm

**[*]Weili CUI, [**]Ronald N. MILES and [***]Quang SU**

Department of Mechanical Engineering,
State University of New York at Binghamton,
Binghamton, NY13902-6000, USA
Tel.: [*]1(607)765-1889, 1(607)777-4620, [**]1(607)777-4038, [***]1(607)777-5286
E-mail: weilicui@yahoo.com, miles@binghamton.edu, quang.su@binghamton.edu

*Received: 28 August 2009 /Accepted: 28 September 2009 /Published: 12 October 2009*

**Abstract:** A novel miniature silicon microphone diaphragm that is highly robust when subjected to residual stress is described [1]. The novel diaphragm is composed of a reinforced plate supported on carefully designed hinges. An approximate model is developed to account for the effects of the small back volume behind the diaphragm and the narrow slits around the perimeter using finite element analysis and analytical equations. The overall dimensions of the polycrystalline silicon diaphragm are 1mm by 1mm by 40 microns. The measured response of the diaphragm closely resembles that of an ideal rigid plate over a frequency range extending well beyond the audible range. This approach leads to a structure that is remarkably robust and tolerant of the stresses that have plagued efforts to fabricate miniature microphones [2, 3]. Potential applications include advanced consumer products such as cell phones, portable digital devices, and camcorders. *Copyright © 2009 IFSA.*

**Keywords:** MEMS, Silicon microphone, Stress, Miniature diaphragm, Fabrication

## 1. Introduction

Residual stress produces major challenges in the fabrication of MEMS devices. This is particularly true in the development of MEMS microphones since the response of the thin sound-sensitive diaphragm is strongly affected by stress. Because the stress is strongly dependent on fine details of the fabrication process that are almost impossible to control sufficiently, it nearly always has significant detrimental effects on microphone performance.

Much effort has been made to control the flatness and dynamic performance of thin film diaphragms

[4-10]. Lee, *et al* [11] discloses a method to fabricate a micromachined pressure transducer having a multi-layer silicon nitride thin film cantilever diaphragm. The technique relies on the symmetry of the stress gradient in the two outer layers and a larger tensile stress (250 MPa) in the second layer to maintain diaphragm flatness. The measured static deflection due to stress is more than 15 microns. This static deflection makes this design unacceptable for miniature capacitive microphones that require a small gap between the diaphragms and back-plates. Loeppert et al. [12] discloses a cantilever center support diaphragm design. A corrugated structure and a sandwich of two quilted films separated by a thin 2-3 micron sacrificial layer are employed to match the diaphragm compliance to the desired pressure range as well as to counter any curling tendency of the diaphragm. It can be difficult to control the flatness with this approach. A patent by Bernstein [13] discloses a structure consisting of a single crystal silicon diaphragm supported on its corners by patterned silicon springs. By supporting the diaphragm only at the corners, it is possible to increase the diaphragm compliance, and subsequently, the sensitivity to sound. This approach permits a design that is more compliant than the usual approach where the diaphragm is supported entirely around its perimeter. However, it does not ensure that the stress in the structure will not result in breakage (if the stress is tensile).

## 2. Design and Fabrication

### 2.1. Diaphragm Design

A robust microphone diaphragm design is presented that maintains good dimensional control under the influence of residual stress, either compressive or tensile, while having its dynamic response dominated by only a single mode of vibration.

This design uses a stiffener-reinforced membrane that is supported on specially designed torsional springs that have very high stiffness in the transverse direction but well controlled stiffness in torsion. The result is a lightweight structure that acts like a rigid plate with a flexible pivot support along one edge. Fig. 1 displays the overall dimensions of the diaphragm.

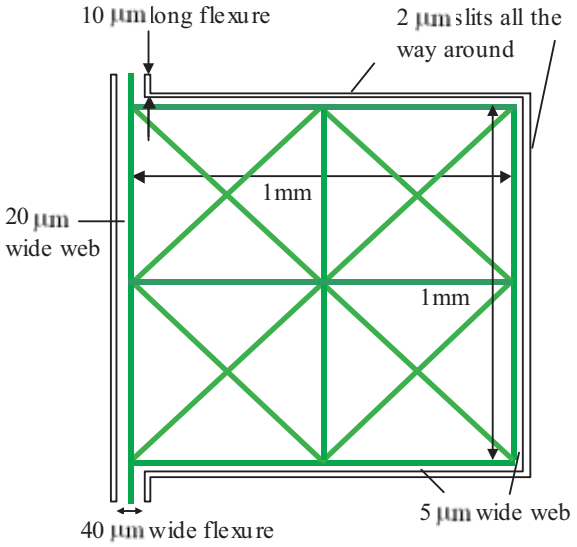


**Fig. 1.** Dimensions of the microphone diaphragm.

The light green represents the 4-micron thick stiffeners that extend 40 microns out of the diaphragm plane. The length of the torsional springs is 10 microns, which has been chosen to tune the structural

stiffness such that the frequency of the first mode is around 24 kHz. Finite element analysis was performed to predict the mode shapes and the effect of the residual stress induced during the fabrication process. Fig. 2 displays the finite element analysis image of the diaphragm. The light blue represents the stiffeners and the purple represents the diaphragm.

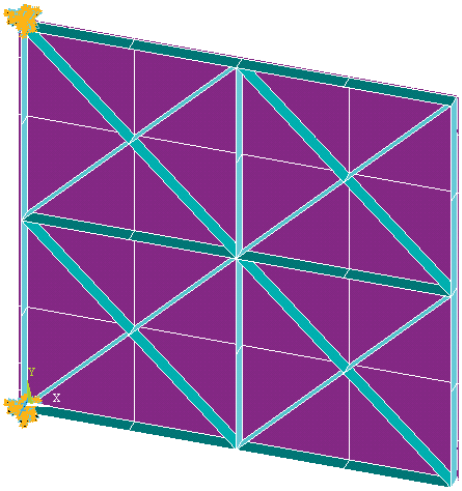

**Fig. 2.** Finite element analysis (ANSYS) image of the microphone diaphragm.

The response of the diaphragm is predicted to be extremely close to that of an ideal rigid plate over a frequency range extending well beyond the audible range. The dynamic characteristics (compliance) of this design can be easily tuned by varying the length of the supporting T section along with its cross sectional dimensions. Assuming that the diaphragm is fabricated out of 2-micron thick polycrystalline silicon and the stiffeners are 4-micron thick and 40-micron tall, the first mode of vibration is predicted to be at 24 kHz (Fig. 3). This mode consists primarily of a rocking motion about the T section supports. Second mode of vibration is predicted to be at 84 kHz consists of twisting motion (Fig. 4). This mode is well above the audible frequency range and thus will not influence the response. By utilizing a stiffened diaphragm structure, the unwanted modes are pushed to ultrasonic frequencies so that the response is very similar to an ideal structure in the frequency range of interest.

Along with having excellent dynamic characteristics, this design concept is highly robust when subjected to stress that may arise during the fabrication process. It is well known that unwanted stress can greatly reduce the yield and the performance of silicon microphones. Because the diaphragm possesses high bending rigidity, it is not prone to buckling when subjected to compressive stress and tends to remain fairly flat under either compressive or tensile stress. The maximum out of plane diaphragm deformation is predicted to be about 0.6 micron when the material is subjected to 40 MPa of isotropic compressive stress as shown in Fig. 5. An identical result, with opposite sign, is obtained for tensile stress. The small deformation shown is substantially less than what would be observed in a conventional design. The maximum stress concentration is about 311 MPa at the corners where the T sections and the web meet. This value is well below the yield stress of polycrystalline silicon which is estimated to be about 1.7 GPa. In addition, the first mode shifts to 24,120 Hz from 24,118 Hz and the second mode shifts to 84,812 Hz from 84,416 Hz with 40 MPa in-plane compressive stress. The dynamic response of the structure is not significantly affected by the stress. The buckling analysis with 40 MPa compressive stress results in an eigenvalue of 4.85 for the first mode, which indicates that the diaphragm will not buckle until the stress reaches 194 MPa (40 MPa times 4.85) [3].

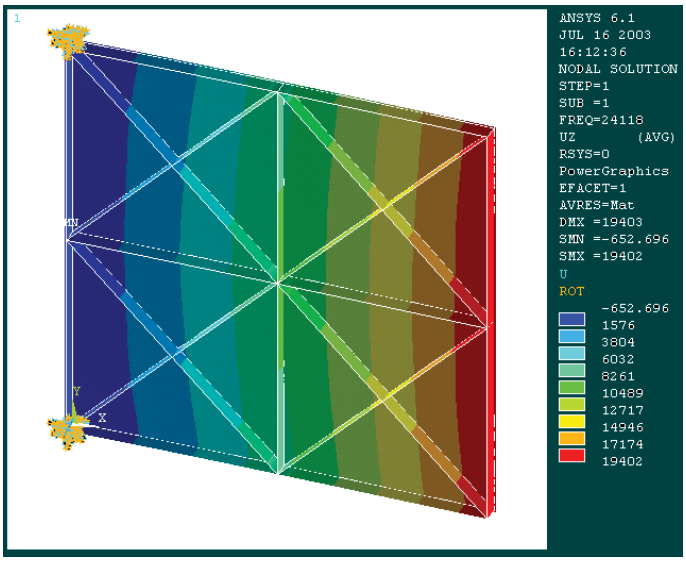


**Fig. 3.** Predicted first mode of vibration of the microphone diaphragm.

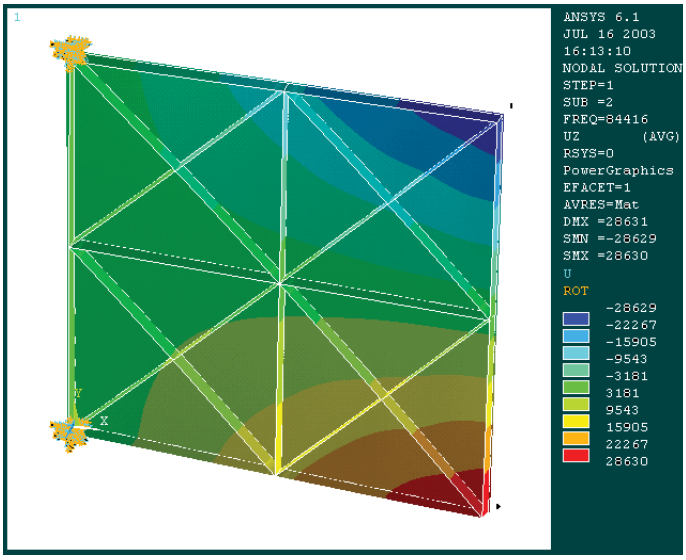


**Fig. 4.** Predicted second mode of vibration of the microphone diaphragm.

## 2.2. Diaphragm Fabrication

The diaphragm fabrication starts with a deep trench etch into the silicon wafer that acts as a mold for the thick polysilicon ribs, followed by sacrificial wet oxide growth and the polysilicon deposition. The oxide layer acts as an etch stop for the backside cavity etch and it also keeps the fragile microphone diaphragm from being fully released following the backside cavity etch. The oxide will hold the membrane firmly in place until it is etched away during the final step. The polysilicon that fills the trenches will become the supporting ribs, and the polysilicon on the surface of the wafer will form the microphone diaphragm or "skin". The polysilicon film is then smoothed with either chemical mechanical polishing or reactive ion etch. The next step is the backside cavity etch that defines the air chamber behind the microphone diaphragm. The wafer is diced into microphone chips before the final microphone diaphragm release.

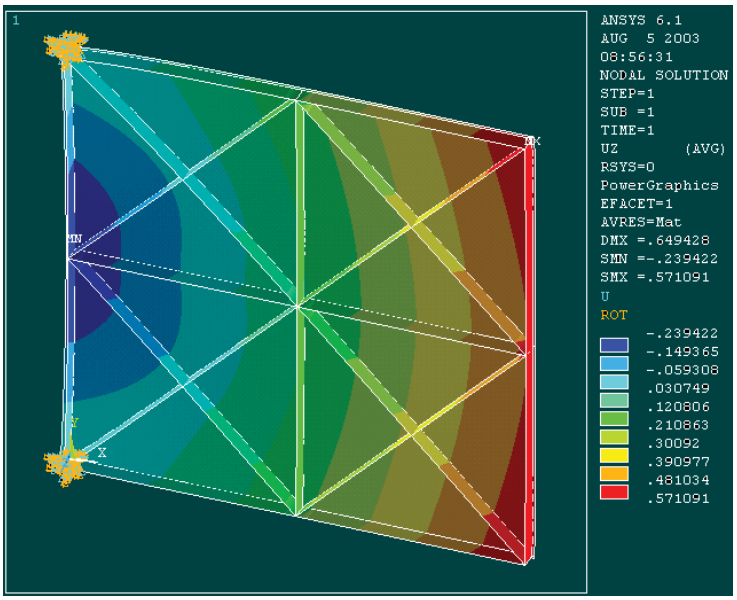


**Fig. 5.** Predicted diaphragm deformation due to 40 MPa of compressive stress.

The microphone diaphragm is then fully released at the chip level by dissolving the sacrificial oxide layer in hydrofluoric acid. Fig. 6 shows the fabrication process flow of the microphone diaphragm [14] and Fig. 7 shows a SEM (Scanning Electron Microscope) image of the vicinity of the hinge support of the fabricated silicon microphone diaphragm.

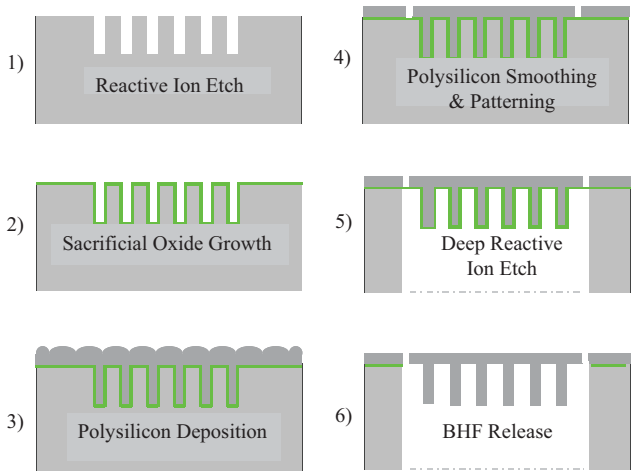


**Fig. 6.** Diaphragm fabrication process flow.

Close examination of the SEM picture of the microphone diaphragm shows that the T-section does not end where the slits end but extends to the wall of the backside etch cavity. And the stiffeners are about 5.45 microns thick instead of 4 microns in the original model, as shown in Fig. 7. A detailed finite element model was constructed to analyze the model and frequency response with the actual parameters and boundary conditions. Fig. 8 shows the finite element model of the vicinity of the hinge support of the diaphragm. The original predicted first two resonant frequencies are 24 kHz and 84 kHz respectively. When the different boundary condition and stiffener thickness are accounted for in the model, the predicted first two resonant frequencies reduce to 17 kHz and 81 kHz respectively.

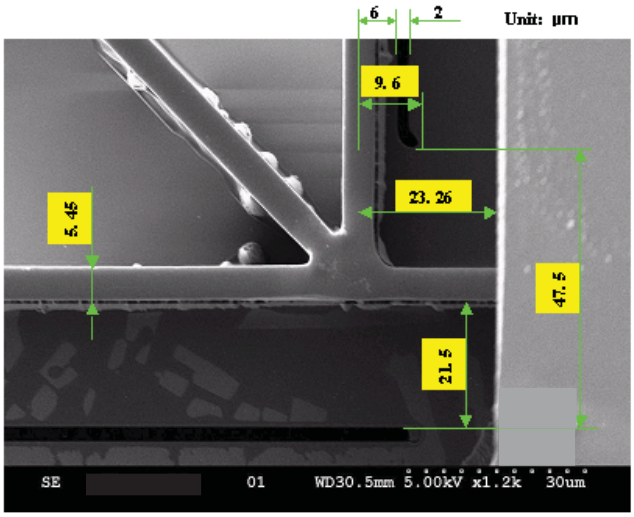


**Fig. 7.** SEM image of the vicinity of the hinge support of the fabricated silicon microphone diaphragm.

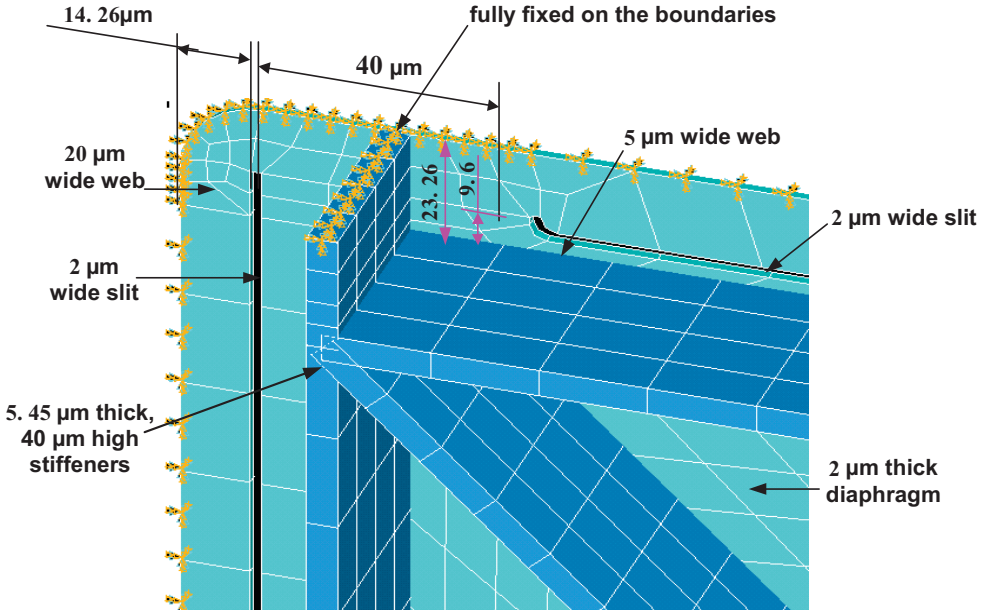


**Fig. 8.** Finite element model of the vicinity of the hinge support of the diaphragm

## 3. Numerical Analysis

### 3.1. Diaphragm with no Slit

For microphone diaphragms with all four edges clamped, only one side of the microphone diaphragm is exposed to the incident sound, the diaphragm response may be modeled as a linear second order oscillator:

$$m\ddot{x} + kx + c\dot{x} = -PA, \tag{1}$$

where m is the diaphragm mass (It may or may not be the actual mass of the diaphragm. Instead, it is the effective or equivalent mass resulting in the correct dynamic response predicted by the lumped mass model), k is the equivalent mechanical stiffness, ***c*** is the viscous damping coefficient, ***P*** is the pressure due to the applied sound field, and ***A*** is the diaphragm surface area. It is assumed that a positive pressure at the diaphragm's exterior will result in a force in the negative direction. If the resonant frequency, $\omega_0 = \sqrt{k/m}$, is above the highest frequency of interest then the mechanical sensitivity will be $S_m = A/k$.

### 3.2. Force Due to Back Volume of Air

If the dimensions of the air chamber behind the diaphragm are much smaller than the wavelength of the sound, we can assume that the air pressure in the volume is independent of location. The air in this volume will then act like a linear spring. The fluctuating pressure in the volume, *V*, due to a fluctuation in the volume, $dV$, resulting from the outward motion of the diaphragm, x, is

$$P_d = \rho_0 c^2 dV / V = -\rho_0 c^2 Ax / V \tag{2}$$

where $\rho_0$ is the density of air and $c$ is the sound speed. The negative sign results from the fact that an outward or positive motion of the diaphragm increases the volume and thus reduces the internal pressure. This pressure in the volume exerts a force on the diaphragm given by

$$F_d = P_d * A = -\rho_0 c^2 A^2 x / V = -K_d x, \tag{3}$$

where $K_d = \rho_0 c^2 A^2 / V$ is the equivalent spring constant of the air in *N/m*.

The force due to the air in the back volume adds the restoring force due to the mechanical stiffness of the diaphragm. Including the air the back volume, equation (1) becomes

$$m\ddot{x} + kx + K_d x + C\dot{x}, = -PA \tag{4}$$

The mechanical sensitivity now becomes $S_m \approx A/(k + K_d x)$.

The small back volume significantly increases the stiffness of the system and causes the viscous flow of air through the slits that separate the diaphragm and the substrate by coupling the air in the slits with the motion of the diaphragm, adding a significant amount of damping. An approximate model has been developed to account for the effects of the small back volume behind the microphone diaphragm and the narrow slit around its perimeter. This is based on a lumped parameter approach where the diaphragm parameters are extracted from the detailed finite element model, and the parameters for the air in the slits and back volume are calculated with theoretical equations. The low-frequency response of the diaphragm is predicted to be adversely affected by the slits and the small back volume. When the back volume and slits are accounted for in the model, there is a 6 dB/octave roll off at low frequencies.

### 3.3. Effect of the Air in the Slit

The air in the slit around the diaphragm will be forced to move due to the fluctuating pressures both within the space behind the diaphragm and in the external sound field. We can again assume that the

dimensions of this volume of moving air are much smaller than the wavelength of sound so that it can be represented by a single lumped mass of mass $m_a$. An outward displacement of the air in the slit, $x_0$, causes a change in volume of the air in the back volume given by $-A_0 x_0$ and a corresponding pressure given by

$$P_{aa} = -\rho_0 c^2 A_a x_a / V, \tag{5}$$

where $A_a$ is the area of the slit on which the pressure acts.

The pressure due to the motion of the air in the slit applies a restoring force on the mass of air in the slit given by

$$F_{aa} = -\rho_0 c^2 A_a{}^2 x_a / V = -K_{aa} x_a, \tag{6}$$

where $K_{aa} = \rho_0 c^2 A_a{}^2 / V$.

The pressure due to the motion of the air in the slit also exerts a force on the diaphragm given by

$$F_{ad} = P_{aa} * A = -\rho_0 c^2 A_a \; A x_a / V = -K_{ad} x_a, \tag{7}$$

where $K_{ad} = \rho_0 c^2 A_a \; A / V$

Likewise, the pressure due to the motion of the diaphragm in equation (2) produces a force on the air in the slit that is given by

$$F_{da} = P_d * A_a = -\rho_0 c^2 A A_a x / V = -K_{da} x, \tag{8}$$

where $K_{da} = K_{ad}$ as given above.

Because the air in the slit is squeezed through a relatively small opening, we must account for the viscous effects which result in a velocity dependent restoring force on the air in the slit,

$$F_{aa} = -c_v \dot{x}, \tag{9}$$

where $c_v$ is a viscous damping coefficient that depends on the details of the flow, as discussed below.

Finally, the externally applied force on the air in slit due to the incident sound field is

$$F_a = P A_a. \tag{10}$$

Summing the forces on the moving elements of the system gives the following pair of governing equations

$$m\ddot{x} + (k + k_d) x + K_{ad} x_a + C\dot{x}, = -PA, \tag{11}$$

$$m_a \ddot{x}_a + k_{aa} x_a + K_{da} x + c_v \dot{x}_a, = -PA_a \tag{12}$$

### 3.4. Response due to Harmonic Sound Fields

If we assume the sound pressure is harmonic with frequency $\omega$ then let $P = Pe^{i\omega t}$. Equation (11) and (12) may be solved to give the steady-state response relative to the amplitude of the pressure. The equations may then be written as

$$\begin{pmatrix} X/P \\ X_a/P \end{pmatrix} = \begin{bmatrix} k+k_d-\omega^2 m+i\omega C & k_{ad} \\ k_{da} & k_{aa}-\omega^2 m_a+i\omega c_v \end{bmatrix}^{-1} \begin{bmatrix} -A \\ -A_a \end{bmatrix} \tag{13}$$

The response of the microphone diaphragm is then

$$X/P = \frac{-A(k_{aa}-\omega^2 m_a+i\omega c_v)+A_a K_{ad}}{(k+k_d-\omega^2 m+i\omega C)*(k_{aa}-\omega^2 m_a+i\omega c_v)-k_{ad}*k_{da}} \tag{14}$$

Note that equation (7) and (8) give $AK_{aa} = A_a K_{ad}$ so that equation (14) becomes

$$X/P = \frac{-A(-\omega^2 m_a+i\omega c_v)}{(k+k_d-\omega^2 m+i\omega C)*(k_{aa}-\omega^2 m_a+i\omega c_v)-k_{ad}*k_{da}} \tag{15}$$

The $\omega$ dependence in the numerator of this expression clearly shows that the response has a high-pass filter characteristic. The cut-off frequency of the high-pass response is given by

$$\omega_{cut} = \frac{k_{aa}k}{c_v(k+k_d)} \tag{16}$$

where we have used the fact that $k_{aa}k_d = k_{ad}k_{da}$.

Note that for a sufficiently large value of $c_v$, equation (15) becomes

$$X/P \approx \frac{-A}{k+k_d-\omega^2 m+i\omega C} \tag{17}$$

in which case the response behaves as if the enclosure is sealed with an equivalent stiffness $k+k_d$.

### 3.5. Diaphragm Acoustic Radiation Loading

If we assume that the microphone diaphragm vibrates like an ideal piston, the results presented above can be modified to account for the radiation load on the piston. The total reaction force on a square piston has been calculated by Morse and Ingard [15]. The force relative to the complex amplitude of the displacement is given by

$$\frac{F_\omega}{X} = \rho c d^2[\omega^2 8d/(9\pi c)+i\omega(\omega d/c)^2/16 \tag{18}$$

where we have assumed the length of each side of the square piston is $d$. Equation (18) can be used to identify a "co-vibrating" mass due to the air near the diaphragm that is given by

$$m_{rad} = \rho c d^2 8d/(9\pi c) \tag{19}$$

One can also identify the frequency-dependent equivalent damping constant due to the radiation,

$$C_{rad} = \rho c d^2 (\omega d/c)^2/16 \tag{20}$$

By including the mass and damping effects of equation (19) and (20), equations (11) and (12) become

$$(m+m_{rad})\ddot{x}+(k+k_d)x+K_{ad}x_a+(C+C_{rad})\dot{x},=-PA \tag{21}$$

$$m_a\ddot{x}_a+k_{aa}x_a+K_{da}x+c_v\dot{x}_a,=-PA_a \tag{22}$$

The response given by equation (15) then becomes

$$X/P=\frac{-A(-\omega^2 m_a+i\omega c_v)}{(k+k_d-\omega^2(m+m_{rad})+i\omega(C+C_{rad}))*(k_{aa}-\omega^2 m_a+i\omega c_v)-k_{ad}*k_{da}} \tag{23}$$

### 3.6. Equivalent Properties of the Microphone Diaphragm

Equation (1) represents the motion of the microphone diaphragm as a simple translating piston with transverse displacement, *x*. It is reasonable to assume that the average displacement of the diaphragm occurs at its center if the pivot occurs along one edge as in the current design. An equivalent lumped mass model in terms of rotation $\theta$, about the pivot may be written as

$$I_{yy}\ddot{\theta}+k_t\theta = PAd/2, \tag{24}$$

where $I_{yy}$ is the mass moment of inertia about the pivot, $k_t$ is the equivalent torsional spring constant, $A$ is the area of the diaphragm that is acting on by the sound pressure $P$, and $d/2$ is the distance between the center of the diaphragm and the pivot. $I_{yy}$ is computed by ANSYS for the diaphragm model to be $I_{yy}$=3.315 $\times 10^{-3}\ kg\mu m^2$. In order to convert the rotational representation of equation (2) into one that uses the displacement $x$ as the generalized coordinate, note that $x=\theta d/2,$ or $\theta = 2x/d$ (small angle approximation). Replacing $\theta$ with $x$ allows us to write equation (2) as

$$I_{yy}2\ddot{x}/d+k_t 2x/d = PAd/2 \tag{25}$$

or

$$I_{yy}(2/d)^2\ddot{x}+k_t(2/d)^2 x = PA \tag{26}$$

Comparing equation (1) and (26) gives the equivalent mass as

$$m = I_{yy}(\frac{2}{d})^2 \approx 1.254\times 10^{-8}\,kg \tag{27}$$

### 3.7. Damping Due to the Slit, $c_v$

Because the slit is only 2 $\mu m$ wide, it is assumed that the flow of air through it is primarily determined by viscous effects. The velocity of the viscous flow in the slit may be approximated by a parabolic profile given by

$$u(y) = -\frac{\partial P}{\partial x}\frac{h^2}{2\mu}(1-(y/h)^2), \tag{28}$$

where $\mu = 1.846\times10^{-5}\, kg/m/s$, and $h = 1\mu m$ is half the distance across the gap. To compute the equivalent viscous damping coefficient we need to relate the net force acting on the air in the gap to the average velocity, $< u(y) >$, where

$$< u(y) >= -\frac{\partial P}{\partial x}\frac{h^2}{2\mu}\frac{1}{2h}\int_{-h}^{h}(1-(y/h)^2)dy = -\frac{\partial P}{\partial x}\frac{h^2}{3\mu} \tag{29}$$

The gradient of the pressure in the slit may be taken as the net pressure on its exterior divided by the depth, $l = 2\mu m$, $\frac{\partial P}{\partial x} = P_{net}/l,$ so that

$$P_{net} = -\frac{3\mu l}{h^2} < u(y) > \tag{30}$$

If the total length of the slit is $w = 4mm$ then the net force is

$$f_{net} = P_{net}\, 2hw = -\frac{6\mu l w}{h} < u(y) > \tag{31}$$

The equivalent dashpot constant is then

$$c_v = \frac{6\mu l w}{h} \tag{32}$$

Since $l = 2\mu m,\ h = 1\mu m,\ w = 4mm,$ and $\mu = 1.846\times10^{-5}\, kg/m/s,$ the dashpot constant due to the slits is $c_v = 8.861\times10^{-7}\, N-s/m.$

### 3.8. Numerical Results

Based on our FEM design model, the static stiffness of the flapping microphone diaphragm $k = 285N/m$. The back volume has dimensions $380\times1012\times1012\mu m^3$. The area of the diaphragm is $A = 1000^2\,\mu m^2$. The width of the slits is $2\mu m$ and the volume of the air in the slits is $V_a \approx 2.9\times10^{-14}\, m^3$ and its mass is $m_a = 3.49\times10^{-14}\, kg$. Equations (3), (6) and (7) then give $K_d = 366N/m, K_{aa} = 0.024N/m,$ and $K_{ad} = 2.97N/m$.

Clearly, $K_d$ and $k$ are the dominant stiffness in the system. The predicted low frequency cut-off of the diaphragm with a closed back volume from equation (16) is 1,923 Hz. The low cut-off frequency

as predicted by equation (16) can be reduced by reducing the stiffness of the diaphragm, $k$. Solving equation (16) for $k$ gives

$$k = \frac{\omega_{cut} c_v k_d}{k_{aa} - \omega_{cut} c_v} \tag{33}$$

If we wish to have a low frequency cut-off of approximately 200 Hz, equation (33) gives a diaphragm stiffness of $k \approx 18 N/m$ [3].

## 4. Microphone Diaphragm Characterization

### 4.1. Experiment Set Up

An experimental setup is described that allows the acoustic response of micro-fabricated microphone diaphragms on bare die to be measured with different back volume configurations. This setup is pictured in Fig. 9. A cylinder fixture with the test die is shown, along with the front lens of a laser vibrometer, a loudspeaker, reference microphone, and microscope. This equipment is mounted on a Newport Research Series vibration isolation table (RS 4000, dimensions 3'x6'x8").

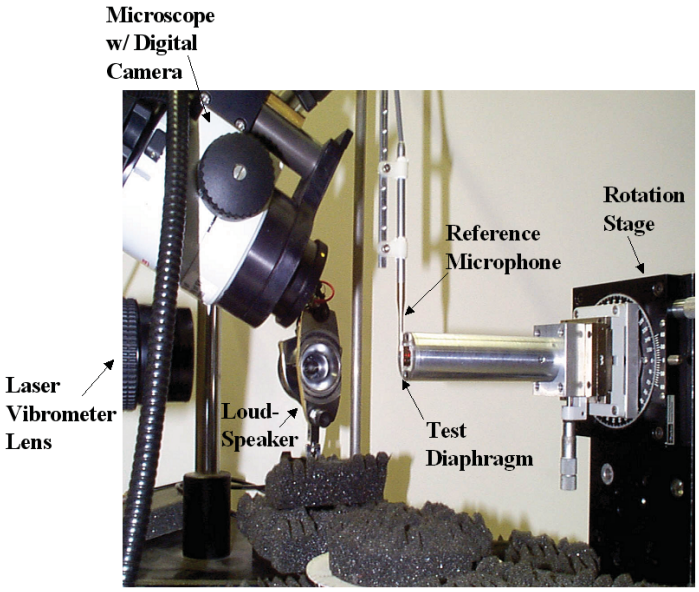


**Fig. 9.** Test setup used to measure the response of the microphone diaphragm.

The microphone diaphragm test die is carefully taped around the edges using wafer tape to attach it to a circular disk (1.25" diameter, 0.07" thick). This disk is bolted to the end of a cylinder (1.25" OD, 0.688" ID, 5" length) that is filled with sound absorbing foam. To test the diaphragm with a large back volume, the chip is mounted to a disk with a $1/8^{th}$ inch (3.175 mm) diameter hole with the test diaphragm centered over the hole, exposing the backside of the diaphragm to the inside of the test cylinder. The diaphragm is tested with a small back volume by mounting the test die on a disk without a hole, making the back volume of the diaphragm defined by the die thickness and backside cavity etch.

A laser vibrometer is used to measure the vibration at the center of the microphone diaphragm (Polytec OFV-302 sensor head with OVF-3000 vibrometer controller). For positioning of the laser spot, the vibrometer sensor head is mounted on a pair of horizontal and vertical Oriel motorized micrometers that are controlled by a joystick (Oriel Motor Mike Control, Model 18000). A dissecting microscope with a digital camera is used to monitor the location of the laser spot as it is manually positioned (Leica Wild M3C, Kodak MDS-100 digital video camera with Optem SC38 microscope attachment). The cylinder is attached to a rotation stage and linear positioning stage to further aid in positioning the test diaphragm relative to the laser vibrometer.

A loudspeaker is placed approximately six inches from the test membrane at grazing incidence to the plane of the test die. The sound pressure generated by the loudspeaker is measured close to the test diaphragm with a 1/8th inch diameter reference microphone, positioned as shown in Fig. 9 (B&K condenser microphone type 4138 with type 2670 pre-amp; B&K dual microphone supply type 5935).

A computer controlled data acquisition system is used to create the excitation signal for the loudspeaker and simultaneously measure the microphone and laser vibrometer signals (Spectral Dynamics, SigLab model 50-21). A burst chirp is sent to a power amplifier that drives the loudspeaker. Data is sampled with 16-bit resolution at 128 kHz. A custom cosine taper window is applied to the laser vibrometer and reference microphone time traces prior to spectral processing to reduce the effects of acoustic reflections. The transfer function of the laser vibrometer with respect to the reference microphone is estimated using 20 spectral averages, then processed to get the mechanical acoustic sensitivity of the diaphragm in units of [mm/Pascal] [14].

### 4.2. Measured and Predicted Frequency Response

Measured and predicted results are shown in Fig. 10 for the response of the center of the microphone diaphragm. The figure shows nearly perfect agreement between our predictions and measurements of the frequency response. When the back volume and slits are accounted for in the model, there is a 6dB/octave roll off at low frequencies as shown in the predicted curves in Fig. 10. The “small back volume” is made up of the 380 microns thick wafer. Measured data were obtained only above 1000 Hz due to the experimental set up. The model we developed does an excellent job in predicting the responses including the low-frequency cut-off effects. The prediction is based on an entirely first principles approach; the model parameters were not adjusted to get the measurements and predictions to agree.

The small back volume and the slits significantly reduce the response of the diaphragm relative to our original prediction, which neglected their effects. To offset some of this loss in sensitivity, it is possible to drill a small hole in the ceramic substrate and package to greatly increase the size of the back volume. This would bring the response much closer to our original prediction. A prediction based on increasing the depth of the back volume from 380 microns to 5000 microns is identified in the figure as “predicted large back volume.”

## 5. Conclusions

The design, fabrication, analysis and characterization of a novel robust microphone diaphragm are described. A numerical model is developed to account for the effects of the small back volume and the slits around the perimeter that significantly reduce the response of the diaphragm. The results are extremely encouraging because it appears that this design is not adversely affected by intrinsic stress in the polysilicon. It has been demonstrated with prototype devices that this design approach avoids the difficulties caused by stress in silicon microphones. This is accomplished by employing structural

analysis and design to develop low-mass diaphragms that can withstand stress induced both during fabrication and operation. The current fabrication results reveal that the idea of fabricating a fairly rigid structure that is supported on specially designed supports can lead to revolutionary improvements in microphone design. This approach leads to a structure that is remarkably robust and tolerant of the stresses that have plagued efforts to fabricate miniature microphones.

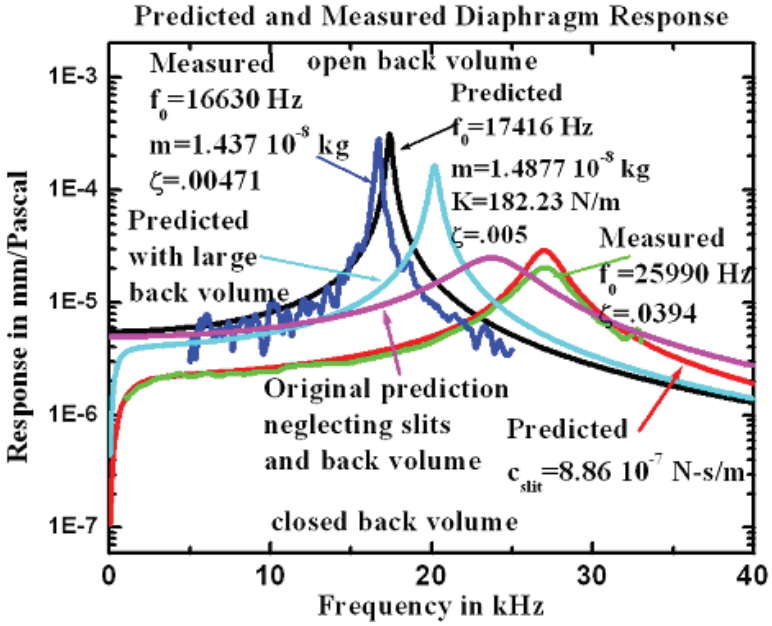


**Fig. 10.** Predicted and measured diaphragm response.

## Acknowledgements

This work is supported by NIH grant 5R01 DC005762-04 (Sensing and Processing for Directional Hearing Aids), 1R01DC009429-01 (Low-Noise Microphone) and 1R01DC009859-01 (Second-Order Microphone) from the National Institute of Deafness and Other Communication Disorders to RNM and partially supported by Binghamton University's New York State Center of Excellence in Small Scale Systems Integration and Packaging through funding from the New York State Foundation for Science, Technology and Innovation (NYSTAR) and Empire State Development Corporation (ESDC).

## References

[1]. W. Cui, R. N. Miles, Q. Su, The design, analysis and fabrication of a novel miniature silicon microphone Diaphragm, *2009 NSTI Nanotechnology Conference and Trade Show*, May 3-7, 2009, Houston, Texas.
[2]. Miles, R. N., and Cui, W., Robust Diaphragm for an Acoustic Device, patent application filed 10/20/2003.
[3]. W. Cui, Analysis, design, and fabrication of a novel silicon microphone, *Ph.D. Dissertation*, Chapter 2, State University of New York at Binghamton, 2004.
[4]. Scheeper, P. R., Olthuis, W. and Bergveld, P., The design, fabrication, and testing of corrugated silicon nitride diaphragms, *Journal of Microelectromechanical Systems*, 3, pp. 36-42.
[5]. Bergqvist, J. and Rudolf, F., A silicon condenser microphone using bond and etch-back technology, *Sensors and Actuators*, 45, 1994, pp. 115-124.
[6]. Zhang, Y. and Wise, K. D., Performance of non-planar silicon diaphragms under large deflections, *IEEE Journal of Microelectromechanical Systems,* 3, 2, 1994, pp. 59-68.

[7]. Jennan, J. H., The fabrication and use of micromachined corrugated silicon diaphragms, *Sensors and Actuators*, A21-A23, 1990, pp. 988-992.
[8]. Lee, S. S., Ried, R. P., and White, R. M., Piezoelectric cantilever microphone and microspeaker, *Journal of Microelectromechanical Systems*, 5, 1996, pp. 238-242.
[9]. Cunningham, B. and Bernstein, J., Wide Bandwidth Silicon Nitride Membrane Microphones, *SPIE Micromachining and Microfabrication Process Technology III*, Austin TX, September 29-30, 1997.
[10]. Spiering, V. L., Bouwstra, S. and Fluitman, J. H. J., Realization of mechanical decoupling zones for package-stress reduction, *Sensors and Actuators*, A, 37-38, 1993, pp. 800-804.
[11]. Lee, Seung, White, Richard and Pisano, Cantilever Pressure Transducer, U. S. Pat. No. 5, 633, 552, May 27, 1997.
[12]. Loeppert, Peter V., Schafer, David E., Miniature silicon condenser microphone, U. S. Pat. No, 5, 870, 482, February 9, 1999.
[13]. Bernstein, Jonathan J., Acoustic Transducer, U. S. Pat. No. 5, 146, 435, September 8, 1992.
[14]. Cui W., Jones S. A., Miles R. N., Degertekin F. L., Hall N., Bicen B., Optical Sensing in a Directional Microphone Inspired by the Ears of the Parasitoid Fly, Ormia Ochracea, in *Proc. of the 19th IEEE Conference on Micro-Electro Mechanical Systems Conference( MEMS' 2006)*, Istanbul, Turkey.
[15]. Morse, P. M. and K. U. Ingard, Theoretical Acoustics, *Princeton University Press*, Princeton, NJ, 1968.

---